Hydrothermal equalibria and ore formation

Alekseyev V.A.[1], Belokhin V.S.[2], Mokhov A.V.[1], Gromyak I.N.[1] Transfer and precipitation of silica during dissolution of basalt. *UDC 550.4.02*

[1]Vernadsky Institute of Geochemistry and Analytical Chemistry RAS, Russia, 119991, Moscow, st. Kosygina, 19, alekseyev-v@geokhi.ru, [2]Lomonosov Moscow State University, Russia, 119991, Moscow, st. Leninskiye gory, 1,

Abstract. After an experiment at 300°C with a block of massive basalt completely immersed in water for four months, the concentration of dissolved silica (*m*) was higher than the solubility of quartz, however, silica precipitation was not observed. In the experiment with a block of massive basalt immersed in water by half, the *m* value was lower than the solubility of quartz, but silica was deposited on the block above the water level in the form of non-crystalline opal, cristobalite opal and quartz. In an experiment with a cylinder of porous basalt half submerged in water, newly formed silica was found not only on the surface, but also inside the upper half of the cylinder (X-ray computed microtomography). The unusual results of the experiments are explained by distillation, which is initiated by the predominant evaporation of a thin, more thermally conductive layer of water at the water–wall–vapor interface and is enhanced by wetting a rough or porous wall with water. Based on the experimental results, it is shown how the action of this mechanism in natural conditions can lead to the formation of agates.

***Keywords**: experiment, basalt dissolution, silica, transfer, precipitation, agate*

Basalts contain the largest, high-quality and numerous deposits of agates, which are banded nodules of fibrous quartz (chalcedony) (Götze et al., 2020; Moxon, Palyanova, 2020). The formation of agates is usually associated with the extraction of silica (SiO_2) from basalts by hydrothermal solutions, the transfer and deposition of SiO_2 in gas bubbles that were formed earlier during the eruption of lavas (Walger et al., 2009). The experiments presented in this paper demonstrate one of the possible mechanisms of agate formation.

Samples of massive or porous basalt immersed in distilled water in whole or in half were heated for 129 days at 300°C in autoclaves. After quenching the autoclaves, the solutions were filtered (pore size 0.05 microns) and analyzed by inductively coupled plasma atomic emission spectrometry (AES-ICP), and the solid phases were studied using an endoscope, scanning electron microscopy (SEM), energy dispersion analysis (EDA), X-ray diffractometry, X-ray computed micro tomography (CT).

The dissolution of massive basalt immersed in water entirely did not lead to the formation of noticeable amounts of new solid phases either on the walls of the autoclave or on the basalt itself, although the concentration of dissolved silica (*m*) was 13.9 mmol/kg (Fig. 1a), which is significantly higher than the solubility of stable quartz (10.5 mmol/kg according to Plyasunov, 2012). The absence of a noticeable amount of secondary silica in this experiment may be due to the formation of a thin leached layer of amorphous silica on the basalt, which restrained further dissolution of the basalt (Techer et al., 2001). The existence of the layer itself could be supported by a high concentration of silica in solution.

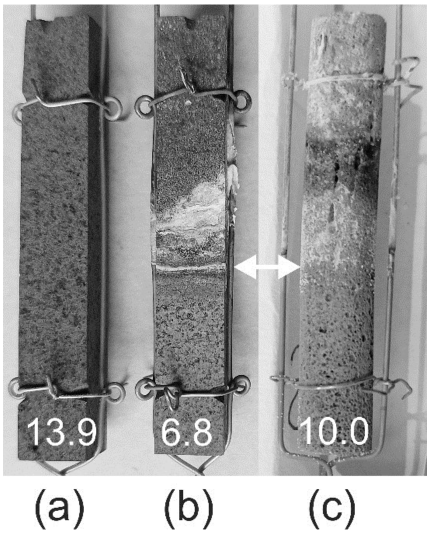

Fig. 1. Photos of basalt samples after runs: massive blocks (1×1×6 cm) submerged in water entirely (a) or half (b) and a porous cylinder (c) submerged in water by half. The white arrows indicate the water level in the experiment. The numbers show the concentration of dissolved silica (mmol/kg) after the run (AES-ICP).

The dissolution of the massive basalt, immersed in water by half, led to the formation of white silica crusts (~100 mg) on the walls of the autoclave above the water level and on the upper half of the basalt itself (Fig. 1b). The newly formed silica is represented by stable quartz and metastable silica modifications (Fig. 2), which have a higher solubility than quartz. All these phases could not be formed directly from the volume of the solution, which was strongly unsaturated relative to quartz (Fig. 1b). Since silica can only be precipitated from a supersaturated solution, in this case there must be an intermediate process of local increase in *m*.

This process is based on the well-known phenomenon of predominant evaporation of a thin (<100 nm) layer of liquid at the edge of the meniscus due to the high thermal conductivity of this layer under conditions of weakened disjoining pressure (Plawsky et al., 2008). The evaporation area increases when a rough or porous surface is wetted with a solution, which increases evaporation. As a result, the concentration in the solution film exceeds the solubility of the solid phase, which precipitates. In a closed system, solution evaporation is compensated by water condensation on other areas of the liquid surface, i.e. distillation takes place in the volume of the solution (Alekseyev, 2023).

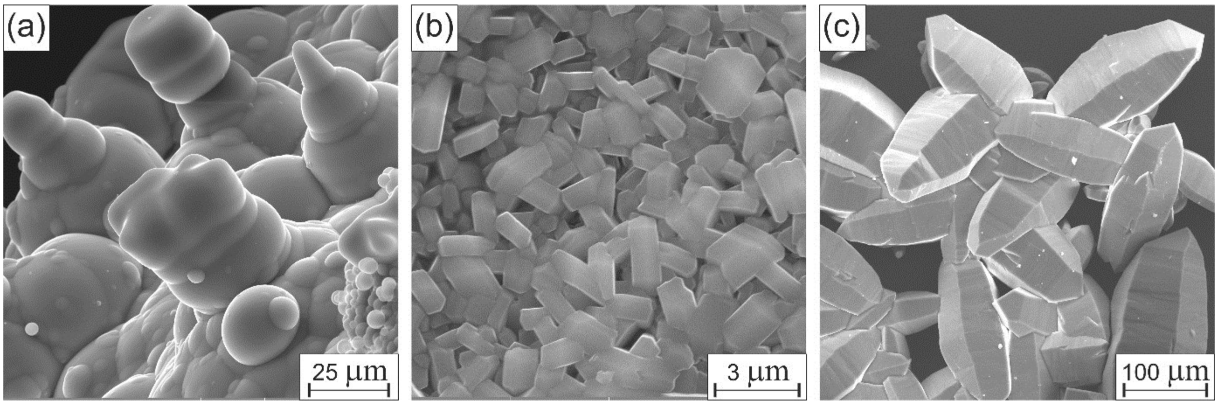

Fig. 2. SEM images of silica phases formed in the upper part of a block of massive basalt half submerged in water (see Fig. 1b): non-crystalline opal-A (a), microcrystalline cristobalite opal-C (b) and macrocrystalline quartz (c). Phase diagnostics: EDA, X-ray, literature data (Graetsch et al., 1994).

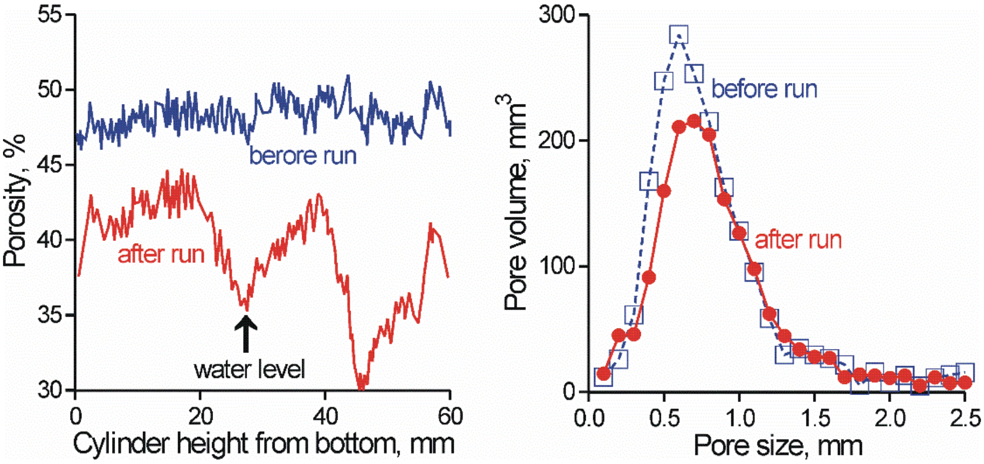

Fig. 3. The porosity profile of the basalt cylinder in height (a) and the pore distribution in this cylinder in size (b) before and after the experiment according to CT data.

According to this hypothesis, basalt partially immersed in water is a long-term nonequilibrium system in which silica passes into the volume of the solution as a result of dissolution of the lower part of the basalt, is transferred in the solution film to the upper part as a result of wetting and precipitates there as a result of evaporation of the film. The duration of silica supply is ensured by the irreversibility of dissolution reactions of primary basalt minerals (plagioclases, pyroxenes, olivines, amphiboles). In these reactions, there is no limitation associated with achieving the equilibrium of minerals with the solution, because minerals formed in the magmatic process become unstable at lower temperatures of the hydrothermal process and must completely dissolve or turn into secondary minerals. Since the main component of basalt is silica, it also becomes the main secondary mineral when basalt is dissolved.

In the experiment with porous basalt half submerged in water, there were few silica crusts on the upper half of the basalt, and they were not visible at all on the walls of the autoclave in an endoscope. The transfer and deposition of SiO_2 occurred by the same mechanism, but mainly inside the pores. As a result, the porosity of basalt decreased after the experiment, and the porosity minima appeared at the water level and above, i.e. in the places of the greatest silica deposition (Fig. 3a). The main bulk of the pores in the basalt cylinder were 0.5-0.8 mm in size (Fig. 3b). It was these pores that reduced their volume in the experiment due to the deposition of silica in them.

The subtraction of combined CT models before and after the experiment in the field of the highest silica deposition allowed us to identify areas of the appearance of silica and the disappearance of basalt (Fig. 4b). A comparison with the tomographic cross section of this site before the experiment (Fig. 4a) showed that silica was formed on the outside of the sample and on the pore walls, and a slight dissolution of basalt occurred on the opposite walls of the pores.

The pores in the basalt were filled with non-crystalline opal-A layers, forming agate-like textures (Fig. 5). The opal-A in places had time to recrystallize into fibrous quartz (chalcedony), i.e. into the main mineral of agates (Fig. 5b). Therefore, opal-A with a multilayer texture on the outside of the basalt sample (Fig. 5c) can be considered as a precursor of agate. According to EDA, chalcedony, unlike opal-A, contained impurities of Al and Na. Replacing Si, these impurities can be the cause of the characteristic features of chalcedony: elongation and twisting of crystals, their spherulite growth (Heaney, Davis, 1995).

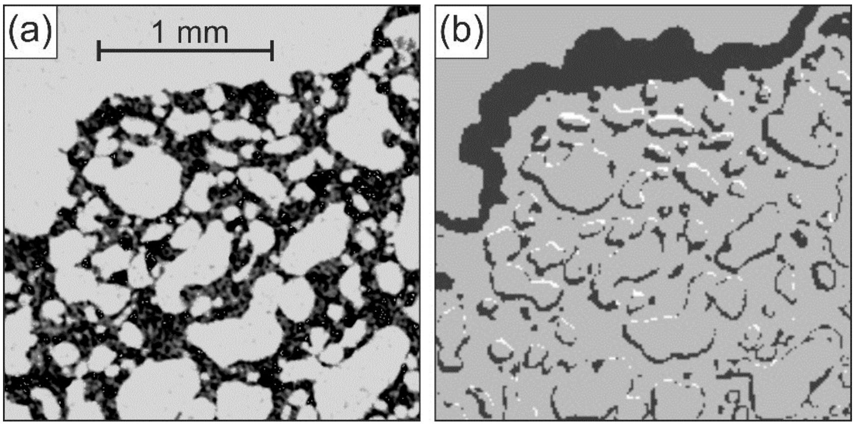

Fig. 4. The edge of the tomographic section of porous basalt above the water level before the experiment (a) and the result of subtracting CT models before and after the experiment in the same section (b). In Fig. (a) the solid phases are dark, the pores are light. In Fig. (b) the areas of appearance of silica are black, the areas of disappearance of basalt are white, unchanged areas are gray).

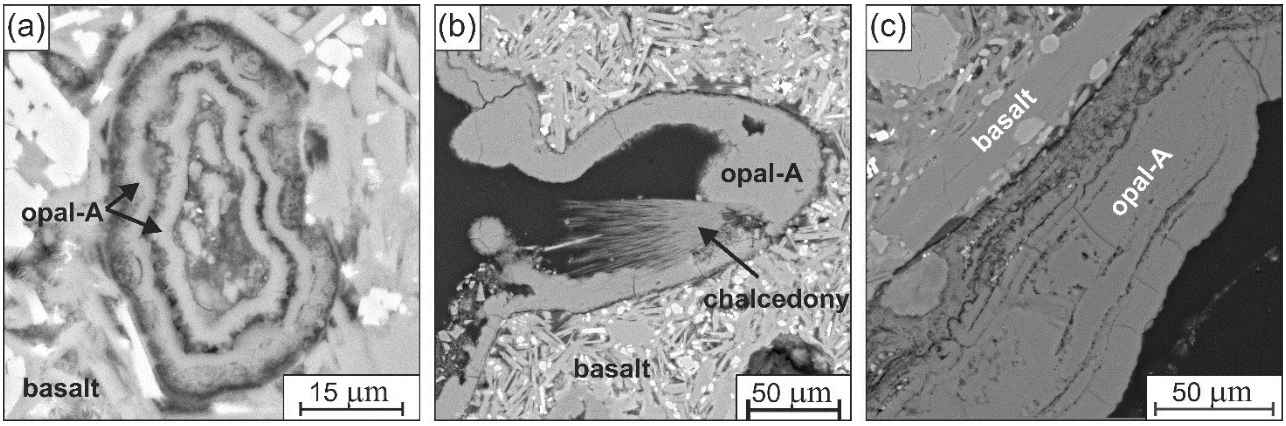

Fig. 5. SEM images of new phases in polished section of the upper part of porous basalt after the experiment: (a) - agate–like texture of opal-A in the pore, (b) – replacement of newly formed opal-A with chalcedony, (c) – multilayer texture of opal-A at the edge of the section. The dark is emptiness.

The described mechanism can manifest itself at a late stage of the hydrothermal process after the heterogenization (boiling) of the fluid with a decrease in T and P (Drummond, Ohmoto, 1985), when the water–vapor boundary is formed and capillary forces arise. Our experiments have shown that evaporation, distillation and wetting accelerate the dissolution of basalt, direct dissolved silica into cavities with a gas phase and deposit silica there in the form of agate-like textures, which over time are able to recrystallize into typical chalcedony agates. The peculiarity of the proposed mechanism of agate formation is that the supersaturation of the solution necessary for solid phase deposition occurs only when solution enters the cavity and begins to evaporate. However, SiO_2 transport to the agate cavity can be carried out in low concentrations, which slows down the deposition of silica in the pores of the host rock and pore blocking. The time required for the formation of agates at 300°C can be many years, and at temperatures <230 °C, more typical for the formation of agates (Götze et al., 2020), a much longer time will be required.

The value of supersaturation of the solution determines the modification of the precipitating silica and the mechanism of its deposition, which, in turn, determines the shape, size and orientation of the crystals, i.e. the texture of the agate layer. Thus, the banding of agates, expressed by quartz layers with different textures, records fluctuations in the supersaturation of the solution from which these layers were deposited. The supersaturation of the film solution may be influenced by: 1) the ratio of wetting and evaporation rates, which depends on the hydrophilicity, roughness and/or porosity of the cavity walls, 2) the ratio of the surface areas of the primary and secondary phases of silica, which changes during transformation reactions of metastable modifications of silica into more stable ones, 3) the SiO_2 diffusion flux from the pore solution of the host rocks, which can change its intensity and configuration due to the processes of primary mineral dissolution and secondary mineral precipitation and also as a result of the evolution of the hydrothermal system itself (a change in T, P, and the composition of the solution).

References

Alekseyev V.A. Spontaneous solution distillation in a closed silica-water system at the water-vapor interface: Review of experimental studies // Advances in Geochemistry, Analytical Chemistry, and Planetary Sciences. (eds. V.P. Kolotov and N.S. Bezaeva). Springer, 2023. P. 175-186.

Drummond S.E., Ohmoto H. Chemical evolution and mineral deposition in boiling hydrothermal systems // Econ. Geol. 1985. Vol. 80, P. 126-147.

Götze J., Möckel R., Pan Y. Mineralogy, geochemistry and genesis of agate – a review // Minerals. 2020. Vol. 10. No 11. art. 1037.

Graetsch H., Gies H., Topalović I. NMR, XRD and IR study on microcrystalline opals // Phys. Chem. Minerals. 1994. Vol. 21. **P.** 166-175.

Heaney P.J., Davis A.M. Observation and origin of self-organized textures in agates // Science. 1995. Vol. 269. No 5230. P. 1562-1565.

Moxon T., Palyanova G. (2020) Agate genesis: A continuing enigma // Minerals. Vol. 10. No 11. art. 953.

Plawsky J.L., Ojha M., Chatterjee A., Wayner Jr. P.C. Review of the effects of surface topography, surface chemistry, and fluid physics on evaporation at the contact line // Chem. Engin. Commun. 2008. Vol. 196. P. 658-696.

Plyasunov A.V. Thermodynamics of $Si(OH)_4$ in the vapor phase of water: Henry's and vapor–liquid distribution constants, fugacity and cross virial coefficients // Geochim. Cosmochim. Acta. 2012. Vol. 77. P. 215-231.

Techer I., Advocat T., Lancelot J., Liotard J.-M. Dissolution kinetics of basaltic glasses: control by solution chemistry and protective effect of the alteration film // Chem. Geol. 2001. Vol. 176. No 1-4. P. 235-263.

Walger E., Mattheß G., Von Seckendorff V., Liebau F. The formation of agate structures: Models for silica transport, agate layer accretion, and for flow patterns and flow regimes in infiltration channels // Neues Jahrb. Mineral. Abh. 2009. Vol. 186. No 2. P. 113-152

Kotelnikov A.R.[1], Suk N.I.[1], Damdinov B.B.[2], Kotelnikova Z.A.[3] Damdinova L.B.[4] Fluids in the earth's crust and their role in the transport of matter (experimental study).

UDC 553.21/24: 550.89

[1]IEM RAS, Chernogolovka, Moscow region; [2]TsNIGRI, Moscow; [3]IGEM RAS, Moscow; [4]IG SB RAS), Ulan-Ude (kotelnik1950@yandex.ru)

Abstract. The report examines the issues of the origin of fluids in the earth's crust, their role in the processes of mineralization and petrogenesis. A review of experimental work on the physicochemical study of various fluid systems at high PT-parameters is provided. The role of fluids in the processes of differentiation of matter under conditions of crustal processes of petrogenesis is shown. The issues of the emergence of a heterophase state are specially considered. Particular attention is paid to the consideration of the following issues: 1) acid-base interaction and distribution of acid and alkaline components in inhomogeneous systems; 2) interaction of fluids with silicate and ore phases and the different effects of acidic and alkaline fluids on melts and mineral phases; 3) solubility of fluid components in melts and behavior of fluid-silicate systems during decompression and decreasing temperature. The complex composition of the ore fluid is emphasized. Using original experimental material, the possibility of modeling the processes of formation of real ore parageneses and developing new criteria for searching for mineral deposits is demonstrated.

Keywords: *fluid, mineralogenesis, petrogenesis, ore phases, differentiation, experiment*

The traditional definition of a fluid is: it is a supercritical aqueous solution in which there is no short-range order in the arrangement of molecules (as in a gas), at the same time, its density is high; the fluid is practically incompressible (like a liquid). A fluid is a special supercritical state of a substance. Fluids play an important role in the processes of endogenous petro- and mineralogenesis. Thanks to fluids, heat and mass transfer occur, various reactions occur in fluid-magmatic systems, and acid-base interaction occurs in heterophase systems. Fluids actively participate in the transport of matter, differentiation and concentration of ore elements. It is believed that there are two main sources of endogenous fluids in the Earth's crust: (1) waterbearing mantle plumes lose water during decompression (both due to the loss of volatiles by melts as pressure decreases, and due to dehydration of the minerals ringwoodite and wadsleyite); (2) the pulling of bound water into the upper mantle in subduction zones due to the mechanism of plate tectonics. The composition of deep fluids is determined by the C-O-H-N system with a small amount (up to 2 wt%) of elements such as sulfur and chlorine. In general, the composition of fluids in a given system is determined by TP-parameters and oxygen potential, so at significant depths with an oxygen buffer IW, a significant amount of hydrocarbons will be present in the fluid, often containing oxygen, chlorine and sulfur. Nitrogen is present in the form of ammonia and hydrocarbon-nitrogen compounds (Sokol et al., 2020). With an increase in oxygen potential, the fluid is oxidized to a dominant content of water, carbon dioxide and nitrogen.

It is generally accepted that the compositions of crustal fluids are mainly modeled by the H_2O-CO_2 system with admixtures of salt components (mainly NaCl). The characteristics of both the pure components of this system (H_2O and CO_2) and the binary H_2O-CO_2, H_2O-NaCl and ternary system H_2O-CO_2-NaCl are examined in detail in experimental works (Kennedy, 1954; Burnham & Holloway, 1969; Sourirajan & Kennedy, 1962; Takenouchi & Kennedy, 1964; Kotelnikova, 2001). Based on the relationship between critical curves and three-phase equilibrium curves, water-salt systems are divided into 2 types. Type 1 is binary systems in which the critical curve does not intersect the three-phase equilibrium curve (example of a system: H_2O-NaCl); Type 2 systems are characterized by the intersection of the critical curve and the three-phase equilibrium curve (example of a system: H_2O-Na_2SO_4). Phase diagrams of systems of types 1 and 2 are discussed in detail in the works of Ravich (1974) and Valyashko (1990).

Mantle fluids enter the lower crust zone at a pressure of about 10 kbar and a temperature of ~1000°C. In this case, partial melting of the lower crust occurs and fluid-magmatic systems are formed. The properties of silicate-volatile systems are described in detail in the works of V.A. Zharikov (1976, 2012). It should be noted that silicate-volatile systems belong to type 2 systems and are characterized by the phenomena of liquid immiscibility. An example of such systems is the H_2O-SiO_2 phase diagram studied in (Kennedy, e.a., 1962). A feature of such systems is the region of liquid immiscibility at high parameters (T~1000°C, P~10 kbar). As the component composition of the system becomes more complex, the phenomena of liquid immiscibility can be observed under other parameters. We modeled liquid immiscibility in trachyrhyolite melts in the presence of excess water during decompression mode (Kotelnikov et al., 2019). Its separation into two silicate liquids is shown, and the separation coefficients of a number of elements between these phases are determined. It has been shown that preliminary accumulation of ore elements can occur in this way. In general, magmatic processes involving volatiles are characterized by the development of liquid immiscibility processes such as silicate melt – sulfide melt, silicate melt – salt melt, silicate melt 1 – silicate melt 2 (differing in composition), silicate melt – metal melt. The phenomena of liquid immiscibility during magmatism processes in connection with ore genesis are discussed in detail in (Suk, 2017; Shapovalov et al., 2019).

When a fluid-saturated magmatic melt rises, it degasses, associated with a decrease in pressure. The separation of the fluid containing salts is accompanied by the hydrolysis of salts and the separation of acidic and alkaline components between the coexisting phases: $NaCl + H_2O = HCl\uparrow + NaOH\downarrow$. In this case, acidic components enrich less dense phases, and alkaline components enrich more dense ones. The processes of acid-base interaction are carried out (Marakushev, Rakcheev, 1982). As a result, the liquid (melt) phase will be alkalized, and the less dense, fluid phase will be acidified. With partial crystallization of the system, the residual melt will become increasingly alkaline. Simultaneously with decompression and separation of volatiles, crystallization of the melt occurs. At high fluid content and pressure of 5-3 kbar, residual water-saturated melts enriched in alkalis can form. Such melts concentrate incompatible elements, including rare ore elements. Residual melts, with a certain decrease in PT-parameters, can gradually transform into a highly concentrated solution enriched with salt, alkaline and ore elements. The existence of such low-temperature solution-melts was modeled by us when studying the system water – potassium fluoride – pyrochlore – quartz at 650-850°C and P = 1 kbar (Shapovalov et al., 2019). It has been shown that the resulting low-temperature silicate solution-melts, enriched with salts (NaF, KF), can concentrate high niobium contents (6-16 wt.% Nb_2O_5).

Binary water-salt systems in which silica or silicates are present belong to the 2nd (P-Q) type, complicated by a metastable region of separation of saturated solutions (Ravich, 1974; Valyashko, 1990). Such systems are characterized by anomalous solubility at elevated PT-parameters, while at low parameters, with increasing temperature, the solubility of metals decreases to a certain point. Studies of type 2 water-salt systems have shown that in the upper region of heterogenization, separation into concentrated brine and weakly concentrated aqueous fluid occurs. The existence of such immiscible fluid phases has been proven by studies of melt and fluid inclusions in the ore-generating granitoids of the Orot and Ermakov beryllium deposits (Damdinov et al., 2023). The transport of matter at the post-magmatic stage is carried out by fluids of complex composition, characterized by alkaline specificity. Their composition is determined by the following salts: NaCl + KCl + Na_2CO_3+ K_2CO_3 + NH_4Cl ± NaF ± KF ± $(Na,K)_2SO_4$. The total salt concentration reaches 30-40 wt%. Under conditions of tectono-magmatic activation, such fluids at a temperature of 450-650°C and a pressure of 2-4 kbar can simultaneously transport ore and silicate substances, forming ore deposits of various types.

Conclusions

1. The fundamental role of fluids in the processes of differentiation of the earth's crust has been determined.

2. Four processes are presented that determine the concentration of ore components: (1) melting of the lower crustal substrate under the influence of mantle fluids; (2) heterogenization of fluid-magmatic systems during decompression (ascent of magmas) with the separation of elements between phases and their accumulation; (3) the stage of crystallization of the magmatic melt in the presence of fluid phases and active acid-base interaction in the system, with the formation of residual melts enriched in ore elements; (4) extraction and redeposition of ore elements by hydrothermal solutions. Combinations of these processes at different PTX-parameters determine the variety of ore deposits.

3. The possibility of experimental modeling of the above processes is shown. Modeling requires accurate knowledge of boundary conditions (parameters of processes in the earth's crust).

The work was supported by the FMUF-2022-0004 program.

References

Burnham C.W., Holloway J.R. The specific volume of water in the range 1000 to 8900 bars, 20 to 900°C. Am.J.Sci. 1969. Schairer. V. 267-A. P. 70-84.

Damdinov B.B., Kotelnikov A.R., Suk N.I., Damdinova L.B., Akhmedzhanova G.M. Experimental modeling of transport of ore-forming components by water-salt fluids at elevated P–T parameters. Russian Geology and Geophysics. 2023. V. 64. N 8. P. 989–1004.

Kennedy G.C. Pressure-volume-temperature relations in CO_2 at elevated temperatures and pressures. Am.J.Sci. 1954. V. 252. P. 225-241.

Kennedy G.C., Heard H.C., Wasserburg G.J., Newton R.C. Upper 3-phase region in system SiO_2-H_2O. Am.J.Sci. 1962. V. 260. P. 501-521.

Kotelnikov A. R., Suk N. I., Kotelnikova Z. A., Yanev Y., Encheva S., Ananiev V. V. Liquid Immiscibility in Fluid–Magmatic Systems: An Experimental Study. Petrology. 2019. V.27. N. 2. P. 186–201.

Kotelnikova Z.A. Synthetic and natural fluid inclusions as a basis for modeling the volatile regime during petrogenesis: Dis. ...Dr. Geol.-Mineral Sciences. M., 2001. 273 p.

Marakushev A.A., Rakcheev A.D. Acid-base properties of chemical elements, minerals, rocks and natural solutions. M., Nauka. 1982. 209 p.

Ravich M.I. Water-salt systems at elevated temperatures and pressures. M., Nauka. 1974. 151 p.

Sokol A.G., Tomilenko A.A., Bulbak T.A., Sokol I.A., Zaikin P.A., Sobolev N.V. Composition of the fluid in the reduced mantle according to experimental data and the results of studying fluid inclusions in diamonds. Geology and Geophysics, 2020. V. 61. N. 5-6. P. 810-825.

Sourirajan S., Kennedy G.C. The system H_2O-NaCl at elevated temperatures and pressures. Am.J.Sci. 1962. V.260. P.115-141.

Shapovalov Yu. B., Kotelnikov A. R., Suk N. I., Korzhinskaya V. S., Kotelnikova Z. A. Liquid Immiscibility and Problems of Ore Genesis: Experimental Data. Petrology. 2019. V. 27. No. 5. P. 534-551.

Suk N.I. Liquid Immiscibility in the Alkaline Magmatic Systems. KDU–Universitetskaya kniga, Moscow. 2017. 238 p.

Takenouchi S, Kennedy G.S. The binary system H_2O-CO_2 at high temperatures and pressures Am.J.Sci. 1964. V. 262. P. 1055-1074.

Valyashko V.M. Phase equilibria and properties of hydrothermal systems. M. Nauka. 1990. 270 p.

Zharikov V.A. Fundamentals of physical and chemical petrology. M. Moscow State University. 1976. 420 p.

Zharikov V.A. Selected works. M., Nauka. 2012. V. 2. 351 p.

Kotelnikov A.R.[1], Suk N.I.[1], Damdinov B.B.[2], Damdinova L.B.[3] Experimental modeling of ore matter transport and formation of ore paragenesis. *UDC 553.062: 550.89*

[1]IEM RAS, Chernogolovka, Moscow region; [2]TsNIGRI, Moscow; [3]IG SB RAS, Ulan-Ude kotelnik1950@yandex.ru

Abstract. Exploratory experiments were carried out to model ore parageneses of the Ozernoye deposit. The experiments were carried out in gold ampoules, into which mixtures of initial aluminosilicate materials with zinc and iron sulfide reagents were loaded, simulating chemogenic precipitation (the lower part of the ampoule). Calcite was loaded into the upper part of the ampoule. The initial solutions (salt concentration up to 45 wt%) were set with chlorides (NaCl, KCl, NH_4Cl) and carbonates (Na_2CO_3 and K_2CO_3). In addition, a small amount of 1M alkali solutions (NaOH, KOH) was added. Solutions of sodium and potassium specificity were used. The experiments were carried out under thermogradient conditions: bottom – 510℃, top – 470℃ and a pressure of 3.5 kbar on an HGPV 10000 installation designed by the IEM RAS. The experimental products were studied using the microprobe method. Using the method of counter-temperature diffusion of components, parageneses similar to natural ones at the Ozernoye deposit were obtained.

***Keywords**: ore parageneses, zinc and iron sulfides, experiment*

Polymetallic (Pb-Zn ± Ag, Cu) sulfide deposits in volcanogenic, terrigenous and carbonate strata provide a significant share of humanity's needs for metals: the predominant quantities, sometimes up to 95%, of Zn, Pb, Ag, Cd, In, Tl, and also significant proportions of Cu, Au, Co, Ni, Se, Te, Ge and Ga (Bortnikov et al., 2016).

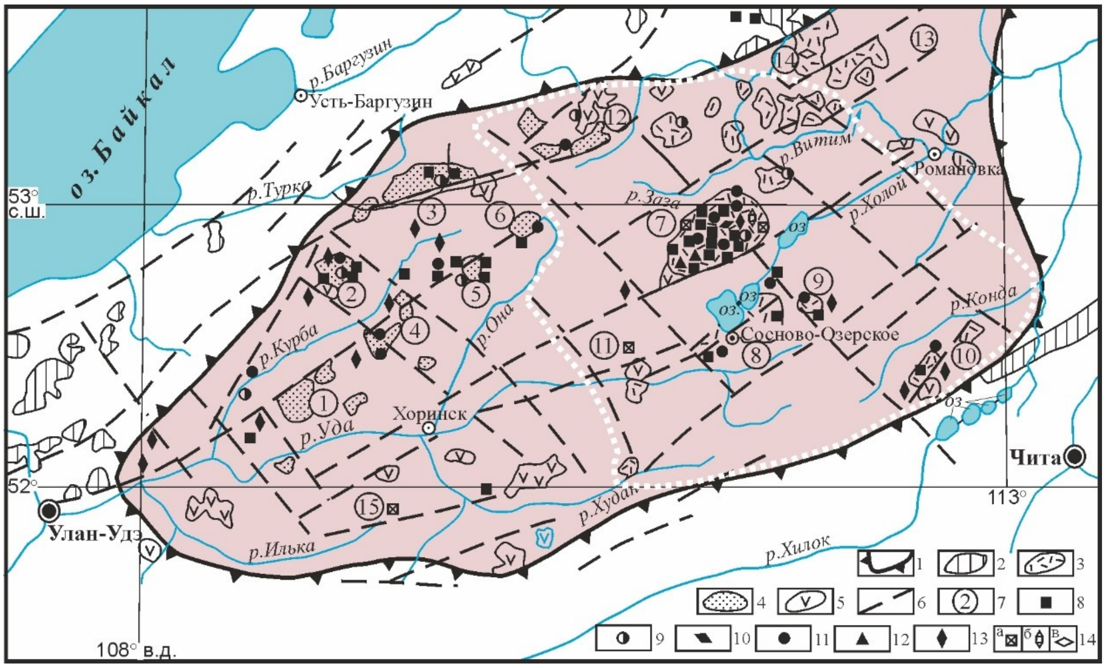

Fig. 1. The layout of ore clusters and minerals of the Kurbino-Eravninsky mineragenic zone and the position of the Eravninsky ore district, according to (Gordienko, Nefediev, 2015) with minor changes.

1 – boundaries of the mineragenic zone; 2–4 – remnants of host rocks among the granitoids of the Angara-Vitim batholith: 2 – Neoproterozoic sedimentary-metamorphic, 3 – Lower Cambrian predominantly carbonate-volcanogenic, 4 – Lower Cambrian and Devonian-Carboniferous terrigenous and essentially carbonate; 5 – Late Paleozoic gabbroid intrusions and xenoliths of mafic rocks among the granitoids of the batholith; 6 – faults; 7 – ore nodes; 8–14 – deposits: 8 – iron, 9 – gold, 10 – manganese, 11 – polymetals (Pb, Zn), 12 – copper, 13 – molybdenum, 14 – fluorite (a), boron (b) and aluminum (c). The white dotted line shows the boundaries of the Eravninsky ore district. The numbers in the circles are ore nodes: 1 – Atkhinsky, 2 – Abaginsky, 3 – Turkinsky (Yambuysky), 4 – Kurbinsky, 5 – Myldylgensky, 6 – Verkhne-Oninsky, 7 – Ozerninsky, 8 – Sosnovo-Ozersky, 9 – Kharasansky, 10 – Kondinsky, 11 – Egitinsky, 12 – Kydzhimitsky, 13 – Khiagdinsky, 14 – Nizhneburulzaysky.

Polymetallic deposits of the Ozerninsky ore cluster are characterized by a complex composition of ores: sulfide mineralization (Pb, Zn), carbonate (siderite), oxide (magnetite) ores. The main part of the ore cluster is composed of stratified Paleozoic formations, making up a remnant (roof sag) with an area of about 250 km^2 in the field of development of Late Paleozoic granitoids of the Angara-Vitim batholith (Fig. 1). The processes of deposit formation and sources of ore matter are still controversial. However, most authors are inclined to metasomatic genesis. Figure 2 shows the geological section of the Ozernoe deposit.

Exploratory experiments were carried out to model ore parageneses of the Ozernoye deposit. The experiments were carried out in gold ampoules, into which mixtures of initial aluminosilicate materials with zinc and iron sulfide reagents were loaded, simulating chemogenic precipitation (the lower part of the ampoule). Calcite was loaded into the upper part of the ampoule. The initial solutions (salt concentration up to 45 wt%) were set with chlorides (NaCl, KCl, NH_4Cl) and carbonates (Na_2CO_3 and K_2CO_3).

In addition, a small amount of 1M alkali solutions (NaOH, KOH) was added. Solutions of sodium and potassium specificity were used in the experiments. The experiments were carried out under thermogradient conditions: bottom – 510℃, top – 470℃ and a pressure of 3.5 kbar. The experiments were carried out on an high gas pressure vessel (HGPV) designed by IEM RAS. The duration of the experiments was 12 days. The experimental products were studied using the microprobe method. Using the method of counter temperature diffusion of components, parageneses similar to natural ones at the Ozernoye deposit were obtained. Of particular note is the synthesis of siderite (Fig. 3), carried out according to the reaction:

$FeS + K_2CO_3(aq) + H_2O + 1.5O_2 \rightarrow FeCO_3 + K_2SO_4(aq)$.

In this way, the genesis of siderite, formed under the influence of alkaline carbonate fluid at an increased oxygen potential, can be explained.

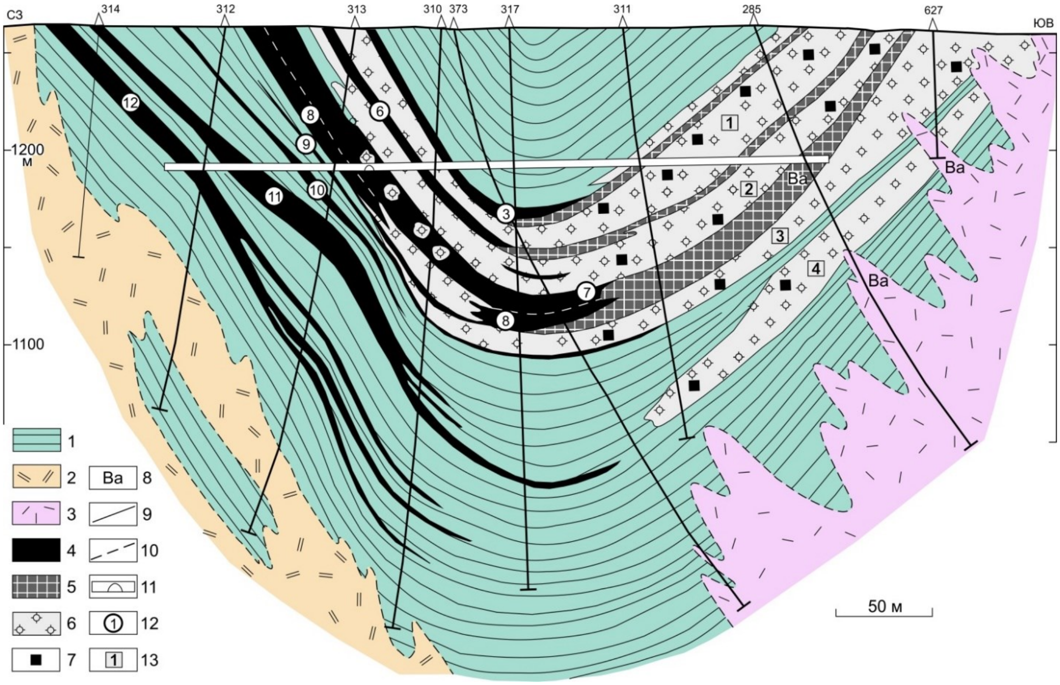

Fig. 2. Schematic geological section of the Ozernoe deposit. 1 – host carbonate-volcano-terrigenous rocks; 2,3 – automagmatic breccias of dacites and andesitodacite (2), rhyolites and rhyodacites (3); 4 – layered bodies of sulfide polymetallic ores; 5 – recrystallized sulfide polymetallic ores; 6 – siderites; 7 – veinlet-disseminated sulfide mineralization; 8 – barite mineralization; 9,10 – geological boundaries established (9) and proposed (10); 11 – mine adit and crosscut; 12,13 – numbers of layered deposits of polymetallic ores (12) and siderites (13).

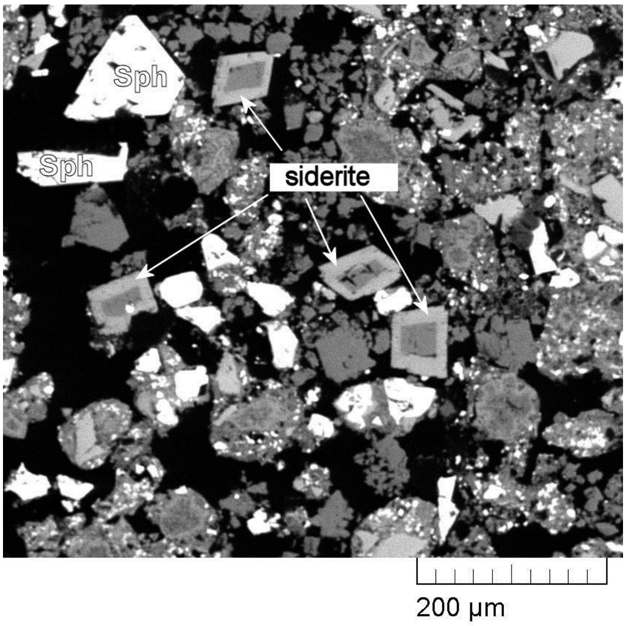

Fig. 3. Siderite (calcite rims) synthesized in experiments of ore substance transport. Sph – sphalerite.

Conclusions

1. Modeling of the formation of parageneses of the Ozernoe deposit under hydrothermal conditions was carried out using the counter-diffusion method at a temperature of 510 - 470℃ and a pressure of 3.5 kbar.

2. The possibility of recrystallization of “chemogenic sediments” enriched in ore components into ore parageneses through metasomatic reactions has been shown.

3. The process of formation of siderites from carbonate-silicate-sulfide substance under the influence of hydrothermal solutions of potassium carbonates was modeled.

The work was supported by the FMUF-2022-0003 program.

References

Bortnikov N.S., Volkov A.V., Galyamov A.L., Vikentyev I.V., Aristov V.V., Lalomov A.V., Murashov K.Yu. Mineral resources of high-tech metals in Russia: status and development prospects. Geology of ore deposits. 2016. V. 58. No. 2. P. 97-119.

Gordienko I.V., Nefediev M.A. Kurbino-Eravninsky ore district of Western Transbaikalia: geological and geophysical structure, types of ore deposits, forecast assessment and development prospects. Geology of ore deposits. 2015. V 57. No. 2. P. 114-124.

Kotova N.P., Korzhinskaya V.S. Comparative analysis of data on pyrochlore and niobium oxide solubility in aqueous fluoride solutions

Korzhinskii Institute of Experimental Mineralogy RAS
Chernogolovka, Moscow district kotova@iem.ac.ru; vkor@iem.ac.ru

Abstract. Experimental data are presented on pyrochlore and niobium oxide solubility in HF, KF solutions in the concentration range of 0.01 - 2 m, in NaF solutions with concentrations of 0.01 - 1 m and in LiF solutions with concentrations of 0.03 - 0.1 m from 300 to 550 °C and 50 to 100 MPa at low oxygen fugacity (Co-CoO buffer). The influence of temperature and pressure on the solubility of Nb oxide and pyrochlore has been established. A comparative analysis was carried out of the niobium equilibrium contents during the dissolution of niobium oxide and natural pyrochlore in fluoride hydrothermal fluids.

Keywords: *experiment, pyrochlore, niobium oxide, fluid, fluoride solutions, physico-chemical conditions*

To model the conditions for the formation of rare metal deposits (Ta, Nb, Be, etc.), in addition to the magmatic factor, it is also necessary to take into account the role of hydrothermal-metasomatic processes. Therefore, we are conducting experimental studies of the behavior of rare metals in aqueous fluids at temperatures and pressures corresponding to the physical and chemical parameters of post-magmatic processes, aimed at obtaining quantitative estimates of the physical and chemical conditions for the formation of greisen and albitite deposits of W, Mo, Sn, Ta, Nb and Li, associated with standard calc-alkaline, including lithium-fluoride granites (Korzhinskaya, Kotova, 2012; Kotova, 2014).

Experimental data on the solubility of pyrochlore $(Ca, Na)_2(Nb, Ta)_2O_6(O, OH, F)$ and niobium oxide (β- Nb_2O_5) in HF, KF, NaF and LiF fluoride solutions are presented, since these are the components that have been established as the main components of fluid inclusions in minerals of rare metal deposits (Webster et al., 2004).

The solubilities of the natural mineral pyrochlore and niobium oxide were studied in solutions of HF, KF with a concentration of (0.01-2.0 m), NaF with a concentration of (0.01-1.0 m) and LiF with a concentration of (0.01-0 ,3 m) in a wide temperature range of 300 – 550^{o} C, P = 50 and 100 MPa and low oxygen fugacity (Co-CoO buffer). For the experiments we used fragments of pyrochlore single crystals from the weathering crusts of the Tatarka carbonatite deposit with the following composition: Na_2O-7,61%; CaO-14,28%; Nb_2O_5-71,61%; F-5,18%; TiO_2-0,83%; Ta_2O_5 ≤1% wt. and niobium oxide in the form of a reagent (special purity grade), pre-purified by recrystallization in 0.1m HF at 550°C and P = 100 MPa. The experiments were carried out on a high-pressure hydrothermal installation in welded platinum tubes using the ampoule technique. Run duration was 15-30 days (Korzhinskaya et al, 2017; Kotova et al, 2022).

To control congruent or incongruent dissolution and to determine chemical composition of newly-formed phases (in case of their detection) the initial materials and solid run products were studied by X-ray diffraction, and electron microprobe analysis (Cam Scan MV 2300 (VEGA TS5130MM).

The quenched aqueous solutions were then analyzed using ICP/MS (Inductively Coupled Plasma Mass Spectrometry) and ICP/AES (Atomic Emission Spectroscopy) for Nb, Ta, Mn, and Fe and admixture elements Ti, W, and Sn.

The results of experiments to study the concentration dependences of the equilibrium niobium content during the dissolution of pyrochlore and niobium oxide HF, KF, NaF and LiF solutions at T = 550^{o} C, P = 100 MPa (Co-CoO buffer) are presented in Fig. 1 (a, b).

Studies have shown that when pyrochlore is dissolved in HF and KF solutions, the equilibrium Nb content increases from $n*10^{-6}$ m in 0.01m HF to $n*10^{-1}$ m in 2m HF, and from $n*10^{-6}$ m in 0.01m KF to $n*10^{-4}$ m in 1m KF. In NaF solutions, the equilibrium Nb content is much lower than in HF and KF solutions, and in 1 m NaF solution it is $n*10^{-5}$ m. It has been experimentally established that the niobium content in LiF solutions is very small and in a 0.1 m LiF solution is $n*10^{-6}$ m. Moreover, with increasing LiF concentration it practically does not change.

The results of the X-ray phase method for analyzing solid experimental products showed that in fluoride solutions, pyrochlore dissolves incongruently with the formation of new phases: oxyfluoride $Na_2Nb_4O_{11}$and crystals of Nb_2O_5 containing titanium (up to 0.56 wt.%) and fluorine (up to 3.88 wt.%).

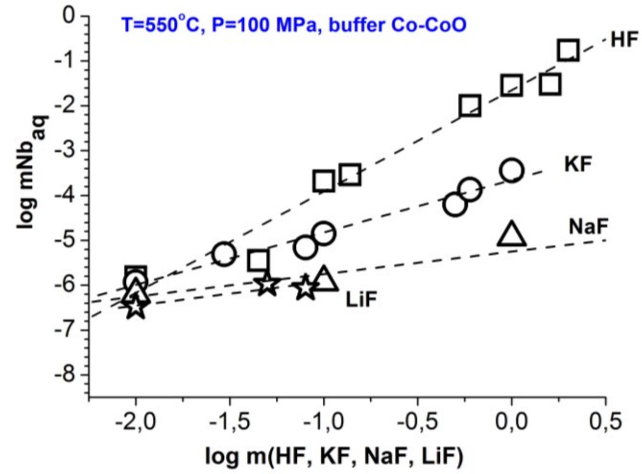

Fig. 1a. Concentration dependence of the equilibrium niobium content during dissolution of natural pyrochlore in fluoride solutions (HF, KF, NaF, LiF) at T = 550°C, P = 100 MPa (Co-CoO buffer)

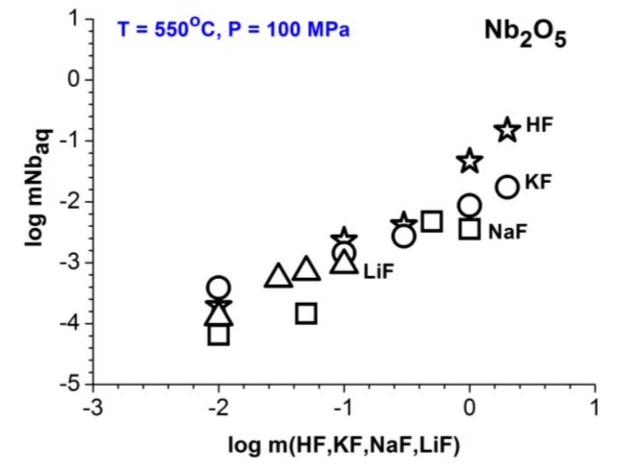

Fig. 1b. Concentration dependence of the equilibrium niobium content during dissolution of niobium oxide in fluoride solutions (HF, KF, NaF, LiF) at T = 550°C, P = 100 MPa (Co-CoO buffer)

According to the experimental data obtained on the solubility of niobium oxide in solutions of HF, NaF, KF and LiF at T = 550 °C, P = 100 MPa (Co-CoO buffer), it was established that the dependence of niobium solubility on fluoride concentration is positive. When niobium oxide is dissolved in fluoride solutions, the equilibrium Nb content increases: from n*10^{-4} m in 0.01m HF to n*10^{-5} m in 2m HF. In solutions of NaF and LiF with a concentration less than 10^{-2} m, the niobium content in the solution is 10^{-4} m. With increasing concentration of fluorine ion, the solubility of Nb_2O_5 increases and at a concentration of NaF 1.0 m, and LiF- 0.1 m, it reaches values of n*$10^{-2.5}$ - n*10^{-3} m, respectively.

The results of the X-ray diffraction method for analyzing solid experimental products showed that Nb_2O_5 is congruently dissolved in 0.1 m HF and LiF solutions. In 1m HF and KF, NaF solutions, niobium oxide dissolves incongruently with the formation of new phases.

Experimental data on the study of the temperature dependences of the equilibrium niobium content during the dissolution of pyrochlore and niobium oxide in 1 m HF, KF solutions at P = 100 MPa (Co-CoO buffer) are presented in Fig. 2 (a, b).

It was found that when pyrochlore is dissolved in 1m solutions of HF and KF, a weak temperature dependence is observed in the temperature range 300-550°C and P = 100 MPa. In 1m HF solutions, the equilibrium niobium content practically does not change with increasing temperature, remaining at the level of n•$10^{-1.2}$ m. In 1m KF solutions, with increasing temperature, the equilibrium niobium content increases by only 1.5 log units: from n•10^{-5} m at 300°C to n•$10^{-3.5}$ m at 550°C.

The study of pyrochlore crystals after experiments using microprobe and X-ray phase analysis methods showed that in a 1m HF solution, pyrochlore dissolves incongruently with the formation of new phases of two types: white needle-shaped crystals with the formula $Na_2Nb_4O_{11}$ and $Nb_{1,98}Ti_{0,02}$ crystals. When pyrochlore is dissolved in a 1m KF solution, the presence of silicon and iron impurities in natural pyrochlore favors the formation of black crystals with the formula $K_3(Nb_3O_6)(Si_2O_7)$, where oxygen is partially replaced by fluorine, the content of which reaches more than 4 wt. %.

It has been experimentally established that when niobium oxide is dissolved in 1m HF solutions, a slight expressed negative temperature dependence of Nb_2O_5 solubility is observed. The niobium concentration has the highest value at T=300°C (n•10^{-1} m), which is only 0.5 orders of magnitude higher than the niobium concentrations obtained for other temperatures. When niobium oxide is dissolved in 1m KF solutions, the equilibrium niobium content is approximately n•10^{-2} m, which is one order of magnitude lower than in 1m HF solutions. The exception is the data obtained at 400°C, where the niobium concentration in a 1m KF solution is n•10^{-3} m, which is one order of magnitude lower than the niobium concentrations obtained for other temperatures.

The results of the X-ray diffraction method for analyzing solid experimental products showed that in a 1m HF solution, over the entire studied temperature range of 300 – 550°C, niobium oxide dissolves incongruently with the formation of crystals of niobium oxyfluoride Nb_3O_7F of the orthorhombic syngony.

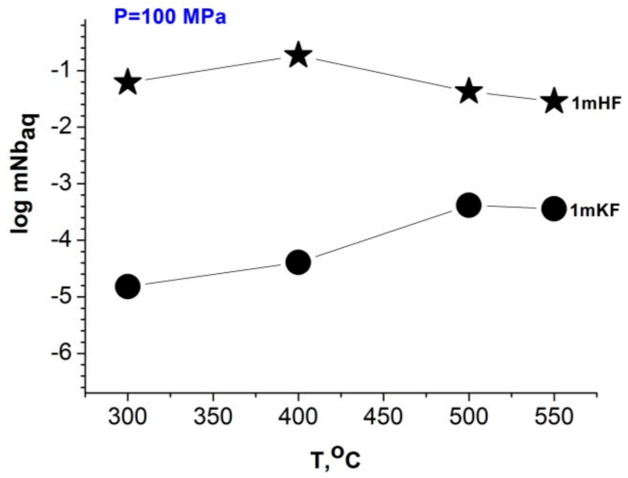

Fig. 2a. Temperature dependence of niobium content during dissolution of pyrochlore in 1 m solutions of HF, KF

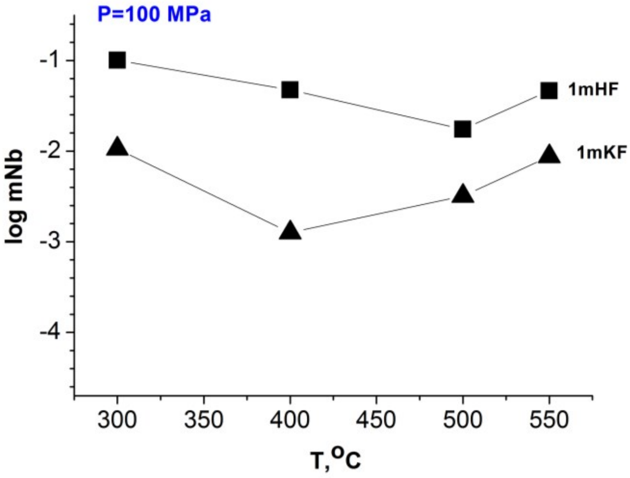

Fig. 2b. Temperature dependence of niobium content during dissolution of niobium oxide in 1 m solutions of HF, KF

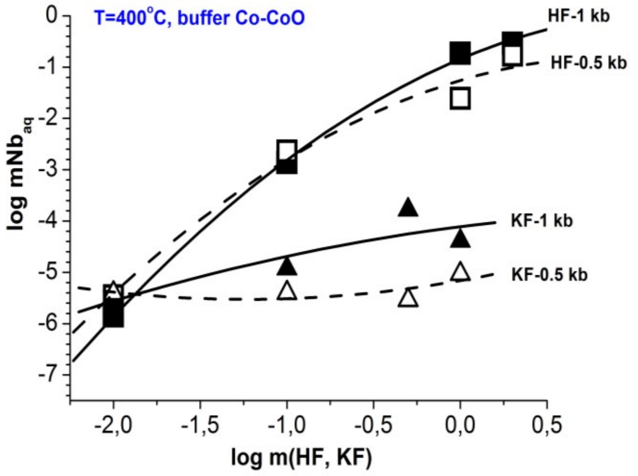

Fig. 3a. Effect of fluid pressure on the solubility of pyrochlore in HF and KF solutions at T = 400°C (Co-CoO buffer)

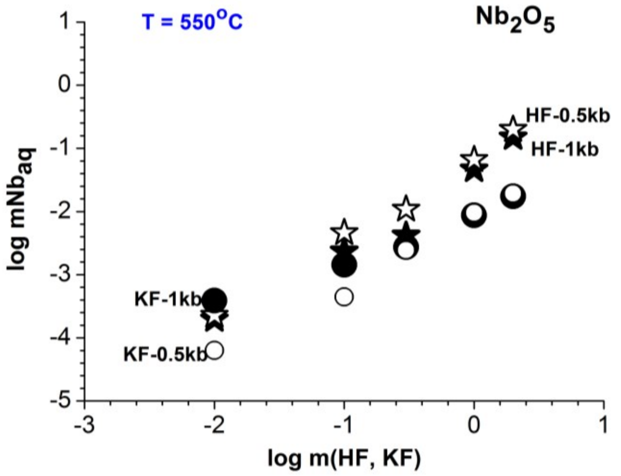

Fig. 3b. Effect of fluid pressure on the solubility of niobium oxide in HF and KF solutions at T = 550°C (Co-CoO buffer)

In a 1 m KF solution at all studied temperatures, crystals of potassium niobate $K_2Nb_4O_{11}$ of the tetragonal syngony are formed.

The conducted studies allow us to conclude that in fluoride solutions of various cationic compositions (HF and KF), the temperature dependence of pyrochlore and β- Nb_2O_5 solubility in the temperature range 300-550° C, P = 100 MPa, Co-CoO buffer is weakly expressed, while as the dependence of solubility on fluoride concentration is strong and positive.

To determine the effect of pressure on pyrochlore and niobium oxide solubilities in aqueous fluoride fluids HF and KF, experiments were carried out at a pressure of 50 – 100 MPa (Fig. 3 a, b).

The diagram (Fig. 3a) shows the results of experiments to study the effect of pressure on the solubility of pyrochlore in HF and KF solutions of various concentrations at T = 400°C and P = 50 and 100 MPa (Co-CoO buffer). It has been established that in HF and KF solutions the effect of pressure on the solubility of pyrochlore is insignificant, especially in the region of low fluoride concentrations. With increasing concentration of fluorides, the niobium content increases by 0.2-0.3 log units. A comparative analysis of data on the solubility of pyrochlore in HF and KF solutions at 400°C showed that the trends of the dependence of the equilibrium niobium content on fluid pressure are identical.

Figure 3(b) shows the concentration dependences of niobium oxide solubility in HF and KF fluids at T = 550°C and pressures of 50 and 100 MPa. It was found that under all studied conditions in HF and KF solutions, niobium oxide has a clearly expressed positive concentration dependence of solubility, which is close to linear in logarithmic units. It has been experimentally established that a decrease in pressure from 100 to 50 MPa in fluoride solutions has practically no effect on the solubility of Nb_2O_5. At low HF concentrations (less than 10-2 m), the niobium content in the solution is at the level of $10^{-3.5}$ m both at P = 100 MPa and at P = 50 MPa. With increasing concentration of F - ion, the solubility of Nb_2O_5 increases greatly and at a concentration of HF- 1.0 m and higher reaches significant values (10^{-2} - $10^{-1.5}$ m). In KF solutions of low concentration, a decrease in pressure leads to a slight decrease in the solubility of Nb_2O_5 by approximately 0.5 orders of magnitude, and with a further increase in the KF concentration, a decrease in fluid pressure has practically no significant effect on the solubility of Nb_2O_5.

Figure 3(b) shows the concentration dependences of niobium oxide solubility in HF and KF fluids at T = 550°C and pressures of 50 and 100 MPa. It was found that under all studied conditions in HF and KF solutions, niobium oxide has a clearly expressed positive concentration dependence of solubility, which is close to linear in logarithmic units. It has been experimentally established that a decrease in pressure from 100 to 50 MPa in fluoride solutions has practically no effect on the solubility of Nb_2O_5. At low HF concentrations (less than 10-2 m), the niobium content in the solution is at the level of $10^{-3.5}$ m both at P = 100 MPa and at P = 50 MPa. With increasing concentration of F - ion, the solubility of Nb_2O_5 increases greatly and at a concentration of HF- 1.0 m and higher reaches significant values (10^{-2} - $10^{-1.5}$ m). In KF solutions of low concentration, a decrease in pressure leads to a slight decrease in the solubility of Nb_2O_5 by approximately 0.5 orders of magnitude, and with a further increase in the KF concentration, a decrease in fluid pressure has practically no significant effect on the solubility of Nb_2O_5.

Comprehensive experimental research on the influence of the bulk concentration of fluoride solutions HF, KF, NaF and LiF, temperature and fluid pressure on the solubility of pyrochlore and niobium oxide can serve as an objective basis for assessing the possibility of niobium mass transfer by hydrothermal solutions in natural conditions, since based on the type of concentration curves obtained under different T-P-fO_2 conditions, one can judge the maximum possible limiting concentration of niobium in aqueous fluid at the early post-magmatic stage after its separation from the crystallizing melt.

The work was carried out on the topic: FMUF-2022-0003

References

1. Korzhinskaya V.S., Kotova N.P. Experimental modeling of the possibility of hydrothermal transport of niobium by fluoride solutions // Bulletin of the ONZ RAS.2012. 4, NZ9001. doi:10.2205/2012NZ_ASEMPG,2012
2. Kotova N.P. Experimental study of Nb2O5 solubility in fluoride solutions at 550oC and 500 bar Experiments in Geosciences. 2014, V.20, N1, pp. 38-39
3. Webster et al., Mineralium Deposita, 2004, V.39, pp. 452-472. doi:10.1007/s00126-004-0423-2
4. Korzhinskaya V. S., Kotova N. P. and Shapovalov Yu. B. Experimental Study of Natural Pyrochlore and Niobium Oxide Solubility in Alkaline Hydrothermal Solutions // Doklady Earth Sciences, 2017, V.475(1), p.p. 793-796. doi: 10.1134/S1028334X17070157
5. Kotova, N.P., Korzhinskaya V.S. and Corresponding Member of the RAS Shapovalov Y.B. Experimental Study of the Solubility of Natural Tantalite and Pyrochlore and Tantalum and Niobium Oxides in Hydrothermal Fluoride–Chloride Solutions // Doklady Earts Sciences, 2022, V. 505(1), pp. 431-438. doi:10.1134/S1028334X22070108

Kotova N.P. Experimental studies of solubility of Nb_2O_5 in LiF solutions at 550°C and 50 to 500 MPa.

Korzhinskii Institute of Experimental Mineralogy RAS,
Chernogolovka Moscow district kotova@iem.ac.ru

Abstract. Experimental data on the niobium oxide solubility in LiF solutions with concentrations of 0.03 and 0.1m at T = 550°C and P = 50, 100, 200 and 500 MPa were obtained. It was found that with an increase in pressure from 50 to 200 MPa, the Nb content in 0.03m LiF solutions practically does not change, remaining at the level of $10^{-3.2}$ mol/kg H_2O. With increase in pressure to 500 MPa, the niobium content decreases to 10^{-4} mol/kg H_2O. In solutions of 0.1 m LiF, when the pressure changes from 50 to 500 MPa, the Nb content decreases from $10^{-2.6}$ mol/kg H_2O to $10^{-3.2}$ mol/kg H_2O. A comparison of the experimental results on the solubility of niobium oxide in LiF solutions showed that at T = 550°C the trends in the dependence of the niobium oxide solubility on the F-ion concentration and fluid pressure are identical.

***Keywords**: experiment, niobium oxide, hydrothermal solubility, pressure, fluoride solutions*

The uniqueness of ore-bearing granites and associated greisen and albitite deposits of rare metals is that in their formation, along with magmatic ones, it is necessary to take into account the role of hydrothermal-metasomatic factors. However, the data available in the literature on the behavior of tantalum and niobium minerals in hydrothermal solutions of various compositions in a wide range of changes in concentration, temperature, pressure and oxygen fugacity are insufficient to understand the role of hydrothermal-metasomatic processes in the genesis of rare metal deposits in granites and assess the degree of reliability of one or another genetic hypotheses. Therefore, we carry out systematic experimental studies of the solubility of mineral phases of tantalum-niobates of complex composition (columbite, pyrochlore, etc.) that are stable in natural conditions, as well as simple oxides of Ta and Nb (Zaraisky et. al., 2010; Korzhinskaya et. al, 2017, Kotova, 2012; Kotova, 2014). The choice of simple Ta and Nb oxides is due to the fact that their solubility limits the upper limit of the concentration of these elements in hydrothermal solutions, since natural minerals that are carriers of Ta and Nb are less soluble than the oxides.

New data have been obtained on the study of the solubility of niobium oxide (β-Nb_2O_5), an analogue of the rare mineral nioboxide, in 0.03 and 0.1 m LiF solutions at 550°C, pressures of 50, 100, 200, and 500 MPa, and oxygen fugacity corresponding to the Co - CoO buffer. The run duration was 10-21 days. Experiments at 550 ° C and 50 to 100 MPa were performed on a hydrothermal line. A sealed-capsule quench technique was employed. Experiments at 550°C and 200 to 500 MPa were carried out on a high gas pressure installation with internal heating (gas bomb). It allows reaching pressures up to 6 MPa and temperatures up to 1400°C. Run temperatures were measured with an accuracy of ± 5°C. The pressure was regulated with a maximum uncertainty of ± 5 MPa.

To control congruent or incongruent dissolution of Nb oxide and to determine chemical composition of newly-formed phases (in case of their detection) the initial materials and solid run products were studied by X-ray diffraction, and electron microprobe analysis (Cam Scan MV 2300 (VEGA TS5130MM).

The quenched aqueous solutions were then analyzed using ICP/MS (Inductively Coupled Plasma Mass Spectrometry) and ICP/AES (Atomic Emission Spectroscopy) for Nb, Ta, Mn, and Fe and admixture elements Ti, W, and Sn.

The results of the experiments are presented in Figs. 1 and 2. Analysis of the data obtained showed that with an increase in pressure from 50 to 200 MPa, the equilibrium Nb content in solutions of 0.03m LiF practically does not change and remains in the range of $n*10^{-3.2}$ mol/kg H_2O. With a further increase in pressure to 500 MPa, the equilibrium niobium content decreases by approximately 0.8 orders of magnitude and amounts to $n*10^{-4}$ mol/kg H_2O. With an increase in the concentration of F^- - ion (0.1m LiF solutions), the equilibrium Nb content increases and at T = 550 ° C and P = 50 MPa reaches a significant value of $n*10^{-2.6}$ mol/kg H_2O. However, an increase in fluid pressure from 50 to 500 MPa in solutions of 0.1 m LiF leads to a decrease in the equilibrium Nb content by 0.6 orders of magnitude: from $n*10^{-2.6}$ to $n*10^{-3.2}$ mol/kg H_2O (Fig. 1).

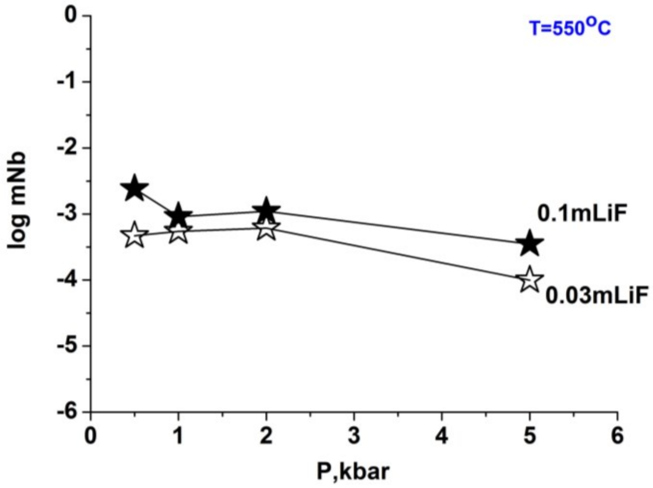

Fig.1. Effect of LiF concentration and fluid pressure on the Nb_2O_5 solubility at T=550°C, Co - CoO buffer (stars – 0.03 m LiF, shaded stars – 0.1 m LiF)

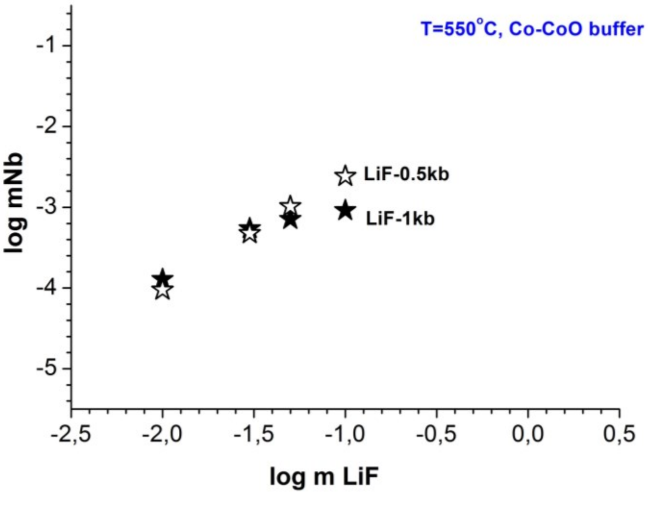

Fig.2. Effect of LiF concentration and fluid pressure on the Nb_2O_5 solubility at T = 550°C, Co-CoO buffer (stars - at P = 0.5 kbar, shaded stars - P = 1 kbar)

A comparison of the experimental results on studying the concentration dependences of the niobium oxide solubility in LiF solutions at T = 550 ° C and a pressure of 50 and 100 MPa showed that under all studied conditions in LiF solutions, niobium oxide has a clearly defined positive dependence of solubility on the fluoride concentration (Fig. 2).

The data presented in Fig. 2 show a generally close and similar dependence of Nb_2O_5 solubility on LiF concentration. Both curves can be well approximated by straight lines having a close slope; the discrepancy in the solubility values of Nb_2O_5 in LiF solutions of different concentrations does not exceed one order of magnitude, which in general allows us to draw a fairly confident conclusion about the decisive role of the F^-- ion in the solubility of Nb_2O_5 and, therefore, about the leading role of complexation of niobium with fluorine.

The results of the X-ray diffraction method for analyzing solid experimental products showed that at T = 550°C and P = 100 MPa in solutions of lithium fluoride of low concentration (0.01 and 0.03 m LiF) niobium oxide dissolves congruently, that is, without changing the composition, and in concentrated solutions of lithium fluoride (0.05 and 0.1 m LiF) niobium oxide dissolves incongruently. In this case, niobium oxide is partially replaced by lithium- niobate $LiNb_3O_8$ At T = 550°C and P = 50 MPa in lithium fluoride solutions of both low and high concentrations, niobium oxide dissolves incongruently with the formation of lithium- niobate crystals $LiNb_3O_8$.

The experimental results obtained can serve as an objective basis for assessing the possibility of niobium mass transfer by hydrothermal solutions under natural conditions, since based on the type of concentration curves obtained, one can judge the maximum possible value of Nb concentration in aqueous fluid at the early post-magmatic stage after its separation from the crystallizing granite melt.

The work was carried out on the topic: FMUF-2022-0003 and with the support of the Russian Foundation for Basic Research (grant 20-05-00307a)

References

1. Zaraisky G.P., Korzhinskaya V.S., Kotova N.P. Experimental Studies of Ta_2O_5 and Columbite-Tantalite Solubility in Fluoride Solutions from 300 to 550 °C and 50 to 100 MPa // J.Mineral and Petrol. 2010. V. 99. N. 3/4. P. 287–300
2. Korzhinskaya V.S., Kotova N.P., and Corresponding member of the RAS Shapovalov Yu.B. Experimental study of natural pyrochlore and niobium oxide solubility in alkaline hydrothermal solution // Doklady Earth Sciences. 2017. V. 475. N.1. P. 793-796.
3. Kotova N.P. Experimental study of concentration dependence of niobium oxide in fluoride solutions at T=550 °C, P = 1000 bar and low oxygen fugacity (Co-CoO buffer) // Experiments in Geosciences. 2012. V.18, N1, P. 123-125
4. Kotova N.P Experimental study of Nb_2O_5 solubility in fluoride solutions at 550°C and 500 bar // Experiments in Geosciences. 2014. V.20. N1. P. 38-39

Novikov M.P., Gorbachev P.N. The influence of P-T parameters on the stability of the rhabdophanit (rabdophan). *UDC 550.4*

Korzhinskii Institute of Experimental Mineralogy RAS
Chernogolovka, Chernogolovka, Moscow district, Russia
novikovi@chgnet.ru

Abstract. The issue of the stability of rhabdophanite-hydrous phosphate of rare earths of the Ce subgroup is of fundamental importance when interpreting the conditions for the formation of rare earth deposits localized in metamorphosed terrigenous strata. Data on the temperature limit of stability of the mineral are very contradictory (Mesbah A., at.al. 2017; Bowles J. 1984; Shelyug A. Mesbah A at all. 2018). Therefore, the task of determining the temperature of the polymorphic transition of rhabdophanite, crystallizing in the hexagonal modification into monazite, which has a monoclinic structure in kinetic terms, was brought to the fore.

***Keywords**: rhabdophanite, solubility, rare earths elements*

Experimental technique. The kinetics of the transition of the hexagonal phase to the monoclinic phase was studied in the temperature range of 500-150°C using the autoclave method. Structural transformations were monitored using X-ray phase analysis. The starting material was aqueous lanthanum phosphate as an analogue of natural rhabdophanite, synthesized in a crystalline state at T = 25°C by precipitation from a lanthanum chloride solution with dilute H_3PO_4. Experiments in a dry system were carried out in hermetically sealed Ni ampoules, which in turn were placed in autoclaves and, therefore, the pressure created in the autoclaves by water was transmitted directly through the walls of the ampoule to the solid phase of aqueous lanthanum phosphate, i.e. water did not interact with the test substance. The volume of the autoclave was 20 cm^3.

Experimental results. A study of the rate of transformation of the hexagonal phase into a monoclinic phase depending on temperature at atmospheric pressure and pressure directly on the solid phase at P = 101.3 MPa using the example of $LaP0_4 \times 0.5H_2O$ – $LaP0_4$ is presented in Fig. 1, 2, 3. Effect of temperature on the duration of the $LaP0_4{\times}0.5H_2O$–$LaP0_4$ phase transition. The numbers in the figures indicate: 1 – hexagonal phase; hex.+mon. phases; 3 – monoclinic phase.

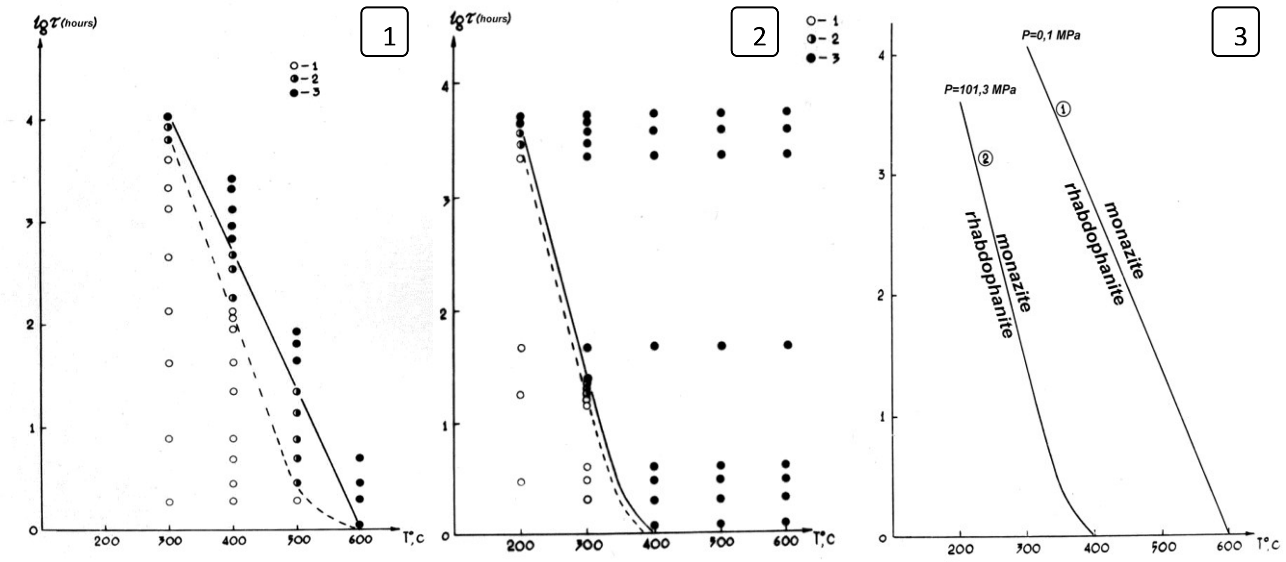

Fig.1. Effect of temperature on the duration of the $LaP0_4 \times 0.5H_2O$–$LaP0_4$ phase transition at atmospheric pressure. **Fig. 2 –** at a pressure of 101.3 MPa (in a dry system)**, Fig. 3—**summarized data from Fig. 1. and Fig.2.

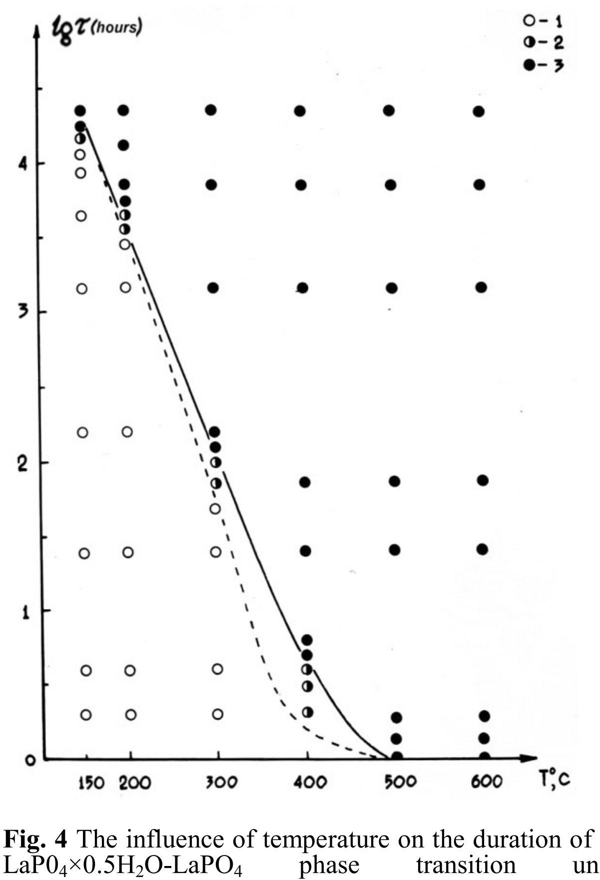

Fig. 4 The influence of temperature on the duration of the $LaP0_4 \times 0.5H_2O$-$LaPO_4$ phase transition under hydrothermal conditions (P_{H2O} = 101.3 MPa).

As can be seen from the presented data, the process of transformation of the hexagonal phase into the monoclinic phase is significantly accelerated when external pressure is applied (Fig. 2, 3) (“dry” system).

Due to the fact that when studying aqueous minerals, it is primarily necessary to take into account factors such as water or water vapor pressure, experiments were carried out to study the influence of H_2O pressure directly on the solid phase (Fig. 4). Here the transformation process proceeds even faster than at the same pressure in a “dry” system. If we take into account that rhabdophanite is a supergene mineral, and water should play an important role in its formation, then based on the obtained material, it becomes obvious that the zeolite type of water in the mineral is not a stabilizing factor in its structure, since its removal according to thermographic analysis is carried out at T=300°C, and the polymorphic transition occurs already at T=150°C.

It should be noted that for all the parameters studied, the conversion of aqueous lanthanum phosphate into anhydrous one occurs only in one direction, i.e. is monotropic. The last factor is of fundamental importance both for the physicochemical analysis of compounds and the conditions for the formation of phosphate rare earth mineralization.

Conclusions. From the experimental data, it can be concluded that rhabdophanite is a metastable mineral and in nature most likely has a chemogenic-sedimentary origin. The process of transition of aqueous phosphate into anhydrous one occurs only in one direction, i.e. is monotropic.

This study is fulfilled under Research program № FMUF 2022-0003 of the Korzhinski Institute of Experimental Mineralogy.

References:

Mesbah A.et al. In pursuit of rhabdophane crystal structure: from the hydrated monoclinic

LnPO4×0.667 H2O to hexagonal LnPO4(Ln=Nd, Sm, Gd, Eu, Dy) // Solid State Chemistry. – 2017. - No. 249. – P. 221-227. Doi: 10.1016/j.jssc.2017.03.004.

Bowles J. The Composition of rhabdophane // Mineralogical magazine. – 1984. – Vol. 48. №1. P. 146-148.

Shelyug A. Mesbah A at all. Thermodynamics and stability of Rhabdophanes, Hydrated rare earth phosphates $REPO_4 \times nH_2O$. // Front. Chem. – 2018. – Vol. 6. P. 604.

Tauson V.L., Lipko S.V., Babkin D.N., Smagunov N.V., Belozerova O.Yu. Origin of Au-Ag mineralization in sphalerite ores: Evidence from hydrothermal study of ZnS-Ag-Au and ZnS-Ag-Au-Sn systems. *UDC 550.89 + 550.42*

A.P.Vinogradov Institute of Geochemistry, Siberian Brunch of RAS (IGC SB RAS), Irkutsk, vltauson@igc.irk.ru

Abstract. The formation of sphalerite with Au and Ag impurities under hydrothermal crystallization of ZnS at 450 °C and 100 MPa pressure was studied. Sn impurity was taken as a source of point defects in crystals modelling the interaction of Au and Ag with vacancies. The Ag solubility in "pure" low-Fe sphalerite is estimated as 3.8±0.7 μg/g, Au – ≤0.6 μg/g. The main forms of Ag and Au occurrence in sphalerite are the inclusions of $(Ag, Au)_xS$ phases with *x* varies mainly from 1.8 to 2.1, and Au varies from 0.01 to 0.75 a.p.f.u. In presence of Sn, the solubilities of Au and Ag become higher. The Au behavior corresponds to the substitution reaction $Sn^{4+} + Au^{+} + v^{-} \leftrightarrow 2\ Zn^{2+}$. Ag entrance is seemingly more dependent on fS_2 conditions and does not correlate with Sn. The elevation of distribution and cocrystallization coefficients are observed for both noble metals (NM), upon that Au changes from incompatible to the category of highly compatible elements in sphalerite. Under real geochemical environments, the evolution of initially "invisible" forms of NM under metamorphic processes and remobilization of ore substance may result in Au and Ag escape and aggregation into microparticles.

Keywords*: hydrothermal systems; sphalerite; silver; gold; tin*

Introduction. The causes and mechanisms of ore substance concentration in objects where it is represented by incompatible elements (noble metals, rare earths, etc.) belong to the most complex and insufficiently studied problems of ore geochemistry. Increasingly widespread studies at the nano-scale (up to the atomic scale) have shown that common views of the state of elements in minerals are not always true, and that fluid-initiated reactions can cause movement from the nano- to micron scale of trace element remobilisation (Cook et al., 2022). Sphalerite is not generally regarded as a gold concentrator, although, for example, it often contains gold, silver and electrum particles in deposits that have undergone remobilisation of ore material from sulphide precipitates formed in ocean floor environments. Observations of visible forms of Au and Ag in ore sulphide assemblages along mid-ocean ridges (MOR) are extremely rare, whereas the existence of "invisible" forms of these NMs in submarine hydrothermal systems has been confirmed by numerous researchers, e.g. (Wu et al., 2016). Micro- and submicroscopic (including nanoparticulate) forms of NM in Zn-rich sulfide precipitates at the outcrops of active hydrothermal systems could be the result of "resetting" of these components, originally represented by impurities trapped on defects (including surface) or regular structural positions of crystallising minerals. This was facilitated by the conditions of rapid deposition of sulfide matter (high defectivity, developed interfacial surface) and increased values of distribution and co-crystallisation coefficients of NM due to the action of duality factors of these coefficients (Tauson et al., 2018). In the present work, experimental modelling of sphalerite formation with Ag and Au impurities during ZnS crystallisation from relatively high-temperature hydrotherms analogous of areas of hydrothermal activity in the MOR and some back-arc spreading centers has been carried out. One of the model systems includes Sn impurity as a possible source of defects in sphalerite, modelling the interaction of NM impurities with vacancies.

Experimental methods and analyses. Experiments were performed using standard hydrothermal thermogradient techniques with internal fluid sampling. The experiment scheme and technical details are given in previous papers (e.g., Tauson et al., 2018). Main parameters of the experiment: temperature in the growth zone 450 ±3° C, temperature drop ΔT - 15° C along the autoclave wall or approximately 2° C in the growth cell (VT-8 titanium alloy liner), PTFC-diagram pressure - 1 kbar, duration 24 days, of which the first 4 days - under isothermal conditions, autoclave quenching in cold running water at a rate of ~ 5 deg/s. Mineralising solution was prepared on the basis of ammonium chloride (concentration - 2 m). In experiments with tin, $SnCl_2$ and $KClO_3$ were added to 2 m NH_4Cl, the latter in order to form SnIV in solution.

The analysis of trapped fluids was performed on atomic absorption spectrometers Perkin-Elmer Model 403, 503 and Analyst 800 (USA) at the IGC SB RAS. The trace elements of interest for the present study were determined with an accuracy of ± 12% and a detection limit of 0.5 ng/ml.

X-ray electron probe microanalysis (EPMA), laser ablation inductively coupled plasma mass spectrometry (LA-ICP-MS) and powder X-ray diffraction analysis (XRDA) were used to analyse the solid products of the experiments. EPMA was performed at the IGC SB RAS on a Superprobe JXA-8200 microanalyser (JEOL Ltd, Japan) equipped with energy-dispersive (EDS) and wave spectrometers (WS). Four to six grains from each experiment were analysed, for a total of 80-100 points per sample; the probe diameter for quantitative analysis with WS was 1 µm. The analysis by LA-ICP-MS method was performed at LIN SB RAS on an Agilent 7500ce instrument with a laser ablation platform New Wave Research UP-213 (USA). The following trace element isotopes were analysed: ^{107}Ag,^{197}Au and ^{118}Sn. The analyses were performed at 20 points of each sample, in 3-4 grains, the laser spot diameter was 55 µm. The calculated detection limits were 0.6 µg/g for each of the above three trace elements. In processing the results of EPMA and LA-ICP-MS methods, we applied the approach proposed earlier for the analysis of Au forms, which involves the formation of criterion-based sampling dataset (CBSD) corresponding to a certain mode of element occurrence (by analogy to statistical samplings of analytical data on single crystals) (Tauson and Lustenberg, 2008). XRDA was performed at the IGC SB RAS on a D8 ADVANCE diffractometer (Bruker, Germany).

Results and discussion. In experiments 1-4, where Sn addition was absent, associations of sphalerite and Au-bearing acanthite with oxidised surface were obtained. Crystals of sphalerite up to 2 mm in size had the usual habitus shapes with the development of faces of two opposite tetrahedrons and a subordinate value of {100}, rarely {110}. In all these experiments two types of sphalerite crystals were present in different ratios - light-coloured, further specimens L, and dark-coloured - specimens D. In experiments with tin (exp. 5 and 6) spherulite-like aggregates of sphalerite up to 1 mm in size were formed; XRDA showed the presence of wurtzite and small amounts of pyrite (exp. 5) and herzenbergite, SnS (exp. 6). The amount of wurtzite did not exceed 15%. According to EPMA data, dark-coloured crystals of sphalerite (D) show, in general, a greater saturation of microinclusions with higher atomic numbers of components compared to L-type samples. Analyses and calculations of the elemental composition of inclusions in sphalerite from exp. 1-4 showed that the main form of Ag and Au inclusions in sphalerite in this system are inclusions of phases $(Ag, Au)_x$ S, in which x varies mainly from 1.8 to 2.1, and less often close to 1, and Au content varies in wide ranges - from 0.01 to 0.75 atom per formula unit. The presence of such inclusions provides a clear correlation of Ag and Au in sphalerite in LA-ICP-MS study (Fig.1). Gold is undetectable in most of the analysis points (≤0.6 µg/g), except for Sn-bearing samples, so it was possible to apply the CBSD procedure for Au only in these latter cases. The situation for Ag is more favourable: the element is detected in all points of analysis (>MDL), although the range of contents is quite significant.

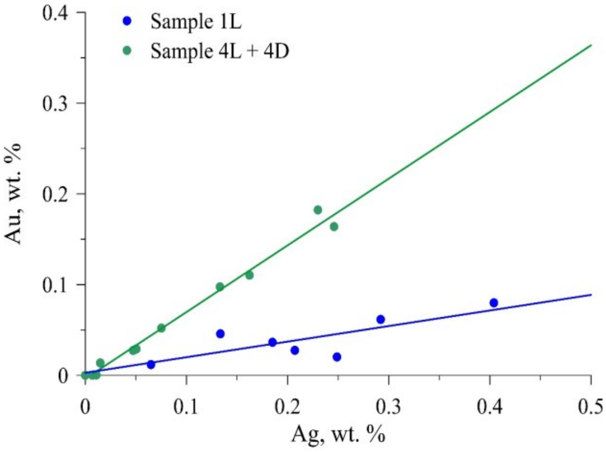

Fig. 1. Correlations between Ag and Au contents in sphalerite in Sn-free systems according to LA-ICP-MS data. Samples from exp. 1 and 4.

This did not prevent us from applying the CBSD procedure and obtaining estimates of the contents of the structural form of Ag in sphalerite: the solubility of Ag in sphalerite at 450° C and 1 kbar was estimated as 3.8±0.7 µg/g based on the results of analyses of three samples from experiments 2-4, for which the relative errors were ±13-21%. According to the available ideas, in the absence of In, Au_2S, native Ag and Ag_2S are considered to be the dominant forms of Au and Ag in sphalerite (Vikentyev et al., 2021). However, according to our data, the primary forms could be $(Ag, Au)_{1.8-2.1}$ S inclusions, and at high fS_2 - (Ag,Au)S inclusions close to equimolar composition. In the sphalerite-wurtzite aggregates of exp. 5 and 6 Au, Ag and Sn are distributed rather homogeneously, positive correlation between Au and Sn concentrations at the analysis points (coefficients of determination 0.6 and 0.7, respectively, Fig. 2) and absence of correlation between Ag and Sn, Ag and Au are observed. In sphalerite, a noticeable decrease in the unit cell edge (to 5.3985 Å) is recorded.

As the analysis of grain stoichiometry by EPMA shows, the behavior of Au in this system, in principle, does not contradict the hypothesis of two types of vacancy defects, namely, non-stoichiometry defects depending on crystallisation conditions and vacancies accompanying the entry of Sn^{4+} into the structure. As shown in Fig. 2, in sphalerite from exp. 6 gold is predominantly associated with vacancies caused by Sn^{4+} incorporation, since at [Sn] = 0 we obtain a value of Au content of 0.3 µg/g, at the level of Au solubility in low-iron sphalerite at 450° C and 1 kbar - 0.7±0.3 µg/g (Tauson and Lipko, 2020). In sphalerite from exp. 5, part of Au is associated with "intrinsic" vacancies, providing an increase of Au solubility in pure sphalerite containing such defects up to 11.4 µg/g (Fig. 2). Such differentiation is confirmed by the EPMA data, according to which the greatest metal deficiency characterises the sphalerite grains from exp. 5. Thus, the behavior of Au is consistent with the scheme $Sn^{4+} + Au^{+} + v^{-} \leftrightarrow 2\ Zn^{2+}$, but silver shows no correlation with Sn and is therefore inconsistent with such a mechanism of incorporation into ZnS. Ag incorporation appears to be more sensitive to fS_2 and it is possible that the presence of vacancy-induced free crystal space favours the formation of AgS or Ag_2S nanoclusters in the structure.

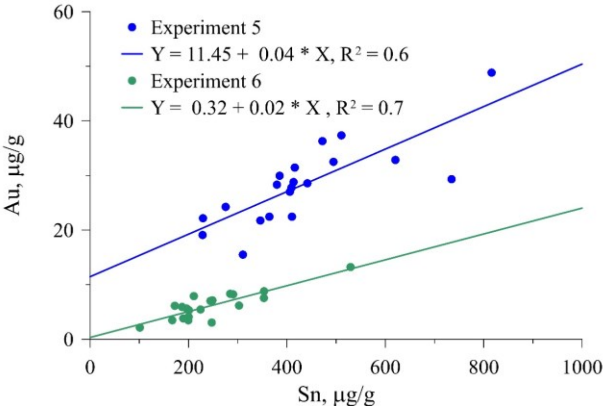

Fig. 2. Au-Sn correlations in tin-bearing sphalerites from experiments 5 and 6 according to LA-ICP-MS data.

According to the data of gold distribution in hydrothermal experiments in multiphase sulfide systems at 450° C and 1 kbar (Lipko et al., 2020), for sphalerite with Fe content ~ 3 wt.% the Au distribution coefficient $D_{Au}^{sph/aq}$ is 0.17±0.04 and Au/Zn $D_{Au/Zn}^{sph/aq}$ co-crystallisation coefficient = $3.6\text{x}10^{-3}$, where *aq* is 5 and 10% solution NH_4 Cl. Comparison of these data with those obtained in the present work indicates the growth of both coefficients in the system with Sn by more than 3 orders of magnitude. Thus, Au passes from the category of strongly incoherent to the category of highly coherent elements in sphalerite. Silver also demonstrates incompatibility in sphalerite in systems without Sn (on average, $D_{Ag}^{sph/aq}$ = 0.1) and a noticeable increase of both coefficients in experiments with tin.

Conclusion. The conditions of formation of highly defective mineral crystals capable of absorbing NM and other elements incompatible in the "ideal" crystal due to their interaction with vacancies and other types of defects can be realised under deposition of massive sulphides in the places where hydrothermal vents exit to the ocean floor in the areas of MOR, hydrothermal fields of island arcs and back-arc basins, and their mixing with seawater at large variations of intense parameters. A similar situation occurs in Irish- and Mississippi Vally- type deposits at high degree of supercooling, oversaturation and rapid reaction between biogenic sulphur and metal-rich fluid. The incorporation of Au and Ag into sphalerite is favoured by supersaturated magmatic fluids and other chemical elements such as In, Ga, Ge and Sn co-deposited with NM. The evolution of these initially "invisible" forms of NM during metamorphism and remobilisation of ore material subsequently leads to the release of Ag and Au aggregating into microparticles. The considered mechanism of NM absorption may be important for understanding the origin and estimation of rare-element potential of ore objects.

The study was carried out within the framework of the state assignment of IGC SB RAS under the FSI Project No. 0284-2021-0002. The equipment of the Centers of Collective Use "Isotope-geochemical studies" of IGC SB RAS and "Ultramicroanalysis" of LIN SB RAS was used in the work.

References

Cook N.J., Ciobanu C.L., Verdugo-Ihl M.R., Courtney-Davies L., Ehrig K., Li W., Liu W., Xu J. Trace elements in minerals: where do we stand on the road between the Holy Grail and a can of worms? // Proceedings of the 16th SGA Biennial Meeting, 28-31 March 2022, Christie A.B. (ed.). Rotorua, NZ, 2022. - V. 1. - P. 65-68.

Lipko S., Tauson V., Bychinskii V. Gold partitioning in a model multiphase mineral-hydrothermal fluid system: Distribution coefficients, speciation and segregation // Minerals. - 2020. - V. 10. - Art. 890.

Tauson V.L., Lipko S.V. Solubility of gold in common gold-concentrating minerals // Russ. Geol. Geophys. - 2020. - V. 61. - No. 12. - P. 1331-1344.

Tauson V.L., Lustenberg E.E. Quantitative determination of modes of gold occurrence in minerals by the statistical analysis of analytical data sampling // Geochem. Int. - 2008. - V. 46. - No. 4. - P. 423-428.

Tauson V.L., Lipko S.V., Smagunov N.V., Kravtsova R.G. Trace element partitioning dualism under mineral-fluid interaction: Origin and geochemical significance // Minerals. - 2018. - V. 8. - Art. 282.

Vikentyev I., Vikent'eva O., Tyukova E., Nikolsky M., Ivanova J., Sidorova N., Tonkacheev D., Abramova V., Blokov V., Spirina A., Borisova D., Palyanova G. Noble metal speciation in hydrothermal sulphides // Minerals. - 2021. - V. 11. - Art. 488.

Wu Z., Sun X., Xu H., Konishi H., Wang Y., Wang C., Dai Y., Deng X., Yu M. Occurrences and distribution of "invisible" precious metals in sulfide deposits from the Edmond hydrothermal field, Central Indian Ridge // Ore Geol. Rev. - 2016. - V. 79. - P. 105-132.